Charged colloids and proteins at an air-water interface: The effect of dielectric substrates on interaction and phase behavior

E. C. Mbamala and H. H. von Grünberg
Fachbereich Physik, Universität Konstanz, 78457 Konstanz, Germany
(Received 23 August 2002; published 26 March 2003)

We study a two-dimensional (2D) system of macroions, trapped at the interface between air and an aqueous electrolyte solution, in the presence of a dielectric substrate approaching the air-water interface from the water side. Working within the linear Debye-Hückel theory, we investigate how the microion-averaged interaction potential between the macroions is affected by the presence of the dielectric substrate. Using these potentials in a Monte Carlo simulation, we further study the changes in the structural and phase behavior of the 2D colloidal system in response to the approaching substrate. Our scope of investigation covers two classes of colloidal particles, namely, highly charged latex particles of tens of nanometers radius, and protein particles of few nanometers radius carrying relatively small numbers of total charge. Probing the bond-orientational order parameter Φ_6 as a function of the 2D particle surface fraction ϕ_{surf} and the air-water–substrate-water separation distance L, our simulations show that structural formations at the air-water interface are strongly influenced by the presence and the dielectric nature of the supporting substrate. Specifically, our $[\phi_{\mathrm{surf}}: L]$ phase diagrams reveal that the transition from the fluid to the crystalline phase is shifted to higher surface fractions, if the approaching substrate is metallic, and to lower surface fractions, if it has a very low dielectric constant. These phase diagrams may be useful for finding materials and substrate interfaces for growing, e.g., 2D crystals of protein particles.

DOI: 10.1103/PhysRevE.67.031608 PACS number(s): 68.43.−h, 82.70.Dd, 87.14.−g, 64.70.Nd

I. INTRODUCTION

The lateral ordering of colloidal particles at interfaces between two different media is of fundamental and practical interest. While it sheds light on the influence of dimensionality on the physics of interaction and phase behavior, two-dimensional (2D) colloidal arrays have also been used—to mention but one practical example—as templates for nanostructuring of solid surfaces [1]. The general interest in 2D colloidal systems has been triggered by the classical work of Pieranski [2] who demonstrated that certain colloids can be trapped at an air-water interface. Since then, observing particles at the air-water interface has been a common and convenient way of investigating 2D or quasi-2D colloidal systems, including studies of clustering and ordering [3,4], aggregation [5–8], collapse of colloidal crystals [9] and foam formation [4,10].

We are interested here in a 2D system of charged colloids at the air-water interface. This system has been studied theoretically by others before [11,12]. Important in our context is the work of Terao *et al.* [11] who have performed Monte Carlo (MC) simulations in 2D, of colloidal particles at the air-water interface at low salt concentration and low surface particle densities. The major result of their work includes finding a two stage melting transition of 2D crystals with the hexatic phase intermediate between the solid and the fluid phases. However, this study may be inconclusive since some of the motivating experiments—including notably the observation of 2D colloidal crystals and clusters [2,3,9], and, more importantly, crystallization of proteins at the air-water interface [13,14]—involve an additional dielectric interface apart from the air-water interface, which has not been considered in Refs. [11,12].

The present paper therefore focuses on the role of this additional surface. We address the question of how the phase behavior of the 2D colloidal system at the air-water interface is affected when the system is further confined by some substrate having different dielectric characteristics (dielectric constant ϵ_3) from that of the suspension. The additional interface is expected to induce effects due to confinement and image charges, depending on the distance L between the air-water and the substrate-water interfaces. This in turn is expected to have consequences on the interaction and thus on the phase behavior of the system. After first deriving a pair-interaction potential that accounts for the additional dielectric substrate (Sec. II), we proceed as in Ref. [11] and systematically probe in Secs. III and IV, also via MC simulation, the effect of the additional substrate-water interface on the phase behavior of the 2D colloidal system. The two key parameters of our simulations are the dielectric constant ϵ_3 of the additional substrate and the distance L. In order to keep the number of variables as small as possible, we consider only three representative substrates, $\epsilon_3=\infty$ (metal), $\epsilon_3=78.3$ (water), and $\epsilon_3=1$ (air), marking the extremes and thus spanning the possible range of changes expected due to the additional substrate.

Two classes of macroionic particles are investigated, namely, highly charged latex particles and small globular proteins carrying only few charges. Modeling proteins as spherical colloids is certainly a rather crude approximation, ''crude'' in the sense that apart from differences in length and time scales between the two classes of particles, protein particles have the extra complexity of anisotropy. However, regarding, e.g., the more general nonspecific physicochemical properties of the 2D systems of charged interfacial particles, the present study of 2D colloid arrays may offer certain in-

sight, particularly into the question whether or not the growing of 2D arrays of proteins can be influenced by an additional dielectric substrate. Indeed, protein particles in solutions have been reported to form various forms of arrays including crystals, at air-water interface with various types of supporting substrate [13–15]. The need to obtain 2D arrays of proteins arises due to the fact that large 3D single crystals are often difficult to obtain, and the subsequent structural analysis by x-ray techniques can be rather time consuming. On the other hand, 2D arrays of proteins if obtained lend themselves to rapid analysis by electron microscopy techniques and requires only small amounts of sample material [16]. Another application of 2D protein arrays, showing the potential usefulness of these systems, is suggested in Ref. [17] where ferritin (a globular protein with iron core) arrays could be used as the component of an ultimate memory device.

From the above-mentioned studies, one understands that the formation, quality, forms and stability of 2D arrays depend largely on the strength of the attractive and repulsive interparticle forces at play. The interaction between particles at air-water interface are governed by (i) lateral capillary forces [18–20], (ii) electrostatic forces [2,11,21,22] for charged colloids, (iii) magnetic forces [23–25] for the case of magnetic particles, and (iv) the short-ranged van-der-Waals forces. We will concentrate exclusively on the second type of interparticle force. While the last two types of forces can be safely ignored in the system under investigation, a word of caution is in order regarding the capillary forces.

The main cause of the lateral capillary forces is the deformation of liquid surface, which is supposed to be flat in the absence of particles. The larger the interfacial deformation created by the particle, the stronger the capillary interaction between them. Hence, the origin of this force is essentially the particle weight. However, capillary forces can persist even for particles of vanishing size and weight, when particles, instead of being freely floating, are partially immersed (immersion capillary forces) in a thin liquid layer on a substrate [26]. The deformation of the liquid surface in this case is related to the wetting properties of the particle surface, i.e., to the position of contact line and magnitude of contact angle, rather than to gravity. Hidalgo-Álvarez and coworkers [27] have, however, shown that for the sizes of latex particles commonly investigated in the literature (particle diameters <1 μm), lateral capillary forces can be neglected. And in the ignorance of any specific wetting properties we can also ignore the immersion capillary forces in this study. Wetting effects are also essential in reducing the total charge on the interfacial particle relative to its value in the bulk due to partial exposition to the low polarizability half space (the air) [28].

We finally remark that 2D systems of particles are also realized and investigated in sandwich geometries [29], in which particles are laterally confined between two dielectric walls. Studies on structural changes corresponding to systems in sandwich geometry abound, see, e.g. Refs. [12,30,31]. The sandwich system though very similar, is subtly different from the scenario of particles trapped at an interface, e.g., air water (where additional dipole-dipole interaction plays a role) in the vicinity of a second substrate, e.g., glass, metal, etc.

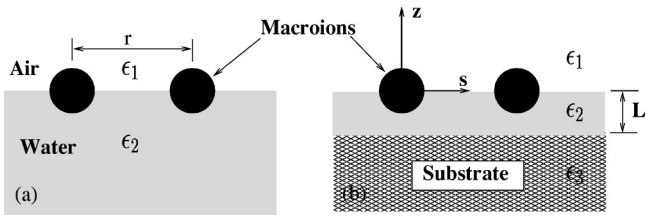

FIG. 1. Two macroions, at a distance r apart, trapped at an air-water interface: (a) no substrate and (b) with a dielectric substrate of separation distance L from the air-water interface.

II. EFFECTIVE PAIR POTENTIALS

We here calculate the electrostatic interaction potential of two point macroions at a distance r apart, each carrying a total number Z of elementary charges e, trapped at the interface formed by a gaseous phase (air) of dielectric constant ϵ_1 (region 1) and an electrolytic solution of dielectric constant ϵ_2 (region 2), see Fig. 1(a). Next we introduce a substrate of dielectric constant ϵ_3 (region 3) such that the electrolyte becomes a quasi-2D film of thickness L [Fig. 1(b)]. Hence, we have three distinct regions resulting in two interfaces; the $\epsilon_1|\epsilon_2$ interface we shall identify as the air-water or air-solution interface, and the $\epsilon_2|\epsilon_3$ interface which will be referred to as the substrate-water or substrate-solution interface, where substrate can be any dielectric material (including air and water) without any mobile or static charges. Only the electrolyte (region 2) is allowed to contain mobile microions, characterized by the inverse Debye screening length κ.

Netz [32] has considered the more general problem in which an electrolytic solution is allowed also in regions "1" and "3" of the slab system. Specifically, he has considered a slab of thickness L, filled in $-L<z<0$ with an electrolyte solution characterized by a screening constant κ_2 and a dielectric constant ϵ_2, and two half spaces, one in $0<z$ characterized by ϵ_1 and κ_1, and another in $z<-L$ with ϵ_3 and κ_3. Within the Debye-Hückel (DH) theory, the electrostatic potential φ at a position $\mathbf{r}$ due to a point test charge Ze located at $\mathbf{r}'$ follows from

$$\frac{k_B T \epsilon_i}{4\pi Z e^2}[\nabla^2-\kappa_i^2]\phi(\mathbf{r},\mathbf{r}')=-\delta(\mathbf{r}-\mathbf{r}'), \tag{1}$$

where $\phi=e\varphi/k_BT$ is the normalized electrostatic potential, with k_BT being the thermal energy. The potential must satisfy Eq. (1) in all three regions ($i=1,2,3$) of the slab system, the three solutions being interconnected through appropriate boundary conditions at $z=-L$ and $z=0$. The problem is rewritten in cylindrical coordinates where $\mathbf{r}\equiv(\mathbf{s},\mathbf{z})$ with $s=\sqrt{x^2+y^2}$, (see Fig. 1), and solved in Fourier space with respect to the lateral coordinate $\mathbf{s}$. Specifying the general solution provided in Ref. [32] to our case at hand ($\kappa_1=0$,

$\kappa_2=\kappa$, $\kappa_3=0$), we obtain the solution for points in the electrolyte medium (region 2), when the test ion is located in the same medium as follows:

$$\phi(s,z,z')=Z\lambda_B\int_0^\infty dk\frac{k}{p}J_0(ks)e^{-p|z-z'|}+Z\lambda_B\int_0^\infty dk\frac{k}{p}\left(\frac{J_0(ks)}{1-\chi_{12}\chi_{23}e^{-2pL}}\right)\times(2\chi_{12}\chi_{23}e^{-2pL}\cosh[p|z-z'|]+\chi_{12}e^{-p(z+z')}+\chi_{23}e^{-2pL}e^{p(z+z')}), \quad (2)$$

where the factors

$$\chi_{12}=\frac{\epsilon_2 p-\epsilon_1 k}{\epsilon_2 p+\epsilon_1 k}, \quad (3)$$

$$\chi_{23}=\frac{\epsilon_2 p-\epsilon_3 k}{\epsilon_2 p+\epsilon_3 k} \quad (4)$$

represent the coupling between the solution and the bounding dielectric media and determine the strength and sign of the image charges. J_0 is the usual spherical Bessel function, $k=|\mathbf{k}|$ is the Fourier conjugate of the real coordinate s, and $p=\sqrt{\kappa^2+k^2}$. $\lambda_B=e^2\beta/\epsilon_2$ with $\beta=1/k_BT$, is the Bjerrum length. We mention that Carnie and Chan [33] have obtained a similar expression for the same problem, but perhaps due to oversight omitted the e^{-2pL} factor in the coefficient of the cosh function in Eq. (2).

The appropriate ion-ion interaction for a pair adsorbed on the interface between medium 1 and medium 2, may readily be obtained from Eq. (2), by setting $z'=0$ and $z=0$, so that $s=r$. The resulting expression provides the value of the potential at distance r along the interface from an adsorbed point ion of total charge Z. The pair interaction is equal to this potential evaluated at the appropriate pair separation, times the charge on the other ion. If both ions have the same charge Z then the pair interaction $\beta U(r,L)$ is

$$\beta U(r,L)=Z\phi(s=r,z=z'=0)=Z^2\kappa\lambda_B\int_0^\infty dl\frac{l}{\tilde{l}}J_0(\kappa rl)\left[1+\left(\frac{1}{1-\chi_{12}\chi_{23}e^{-2\kappa L\tilde{l}}}\right)\times(2\chi_{12}\chi_{23}e^{-2\kappa L\tilde{l}}+\chi_{12}+\chi_{23}e^{-2\kappa L\tilde{l}})\right], \quad (5)$$

where we let $k=\kappa l$ so that $p=\sqrt{\kappa^2+\kappa^2l^2}=\kappa(1+l^2)^{1/2}$ and $\tilde{l}=(1+l^2)^{1/2}$. It can be seen immediately that in the limit of large L in which the problem reduces to that of only one interface formed by media 1 and 2, Eq. (5) reduces to the form obtained by Stillinger [34], namely,

$$\beta U(r,L\to\infty)=2Z^2\kappa\lambda_B\epsilon_2\int_0^\infty\frac{lJ_0(\kappa rl)}{\epsilon_2\tilde{l}+\epsilon_1 l}dl. \quad (6)$$

The same is not true of the expression derived in Ref. [33], due to the ommission pointed out.

We now wish to write Eqs. (5) and (6) for various values of χ_{12} and χ_{23} corresponding to various systems of interfaces in the slab geometry, and for finite and infinite slab thickness L. We will consider only the following representative cases; the air-water only, the air-water-metal, the air-water-air, and the air-water-water systems with the following acronyms; AW, AWM, AWA, and AWW, respectively.

Case I: Air-water only (AW) system. Here the appropriate pair interaction $\beta U^{\rm aw}(r)$ results from Eq. (6), with $\epsilon_1=1$ and $\epsilon_2=78.3$. As Hurds [21] has shown, Eq. (6) can be separated into an exponential and algebraic decaying terms

$$\beta U^{\rm aw}(r)=\beta U^{\rm yuk}+\beta U^{\rm Int}, \quad (7)$$

where the first term

$$\beta U^{\rm yuk}=2Z^2\kappa\lambda_B\int_0^\infty\frac{lJ_0(\kappa rl)}{\sqrt{1+l^2}}dl=2Z^2\kappa\lambda_B\frac{e^{-\kappa r}}{\kappa r} \quad (8)$$

is the familiar Yukawa potential with a factor of 2, and the second term is

$$\beta U^{\rm Int}=-2Z^2\kappa\lambda_B\int_0^\infty\hat{l}J_0(\kappa rl)\left(\frac{\epsilon_{12}\hat{l}}{1+\epsilon_{12}\hat{l}}\right)dl, \quad (9)$$

with $\hat{l}=l/\tilde{l}=l/(1+l^2)^{1/2}$ and $\epsilon_{12}=\epsilon_1/\epsilon_2$. A numerical analysis of the integral, Eq. (9) shows that it grows from weakly negative values at very small pair separations to a positive maximum and decays algebraically to zero at large pair separations. The net interaction potential in Eq. (7), however, remains repulsive for all range of interactions.

Case II: Air-water-metal (AWM) system. We first consider an approximate limiting case where $\chi_{12}=1$ and $\chi_{23}=-1$. From Eqs. (3) and (4), these values correspond respectively, to $\epsilon_{12}=\epsilon_1/\epsilon_2=0$, an approximation of an air-water interface and $\epsilon_{32}=\epsilon_3/\epsilon_2=\infty$ for a metallic substrate-water interface. From Eq. (5), the resulting pair potential $\beta U^{\rm lim}$ is

$$\beta U^{\rm lim}(r,L)=2Z^2\kappa\lambda_B\int_0^\infty\hat{l}J_0(\kappa rl)\tanh(\kappa L\tilde{l})dl. \quad (10)$$

We see immediately that the approximation $\epsilon_{12}=0$ is crude enough to kill the second term in Eq. (7), i.e., Eq. (9), leaving the system with only the Yukawa interaction, Eq. (8). We will hence avoid this approximation, i.e., $\chi_{12}\neq1$, in our pair potentials. Then from Eq. (5) again, the appropriate pair interaction for the air-water-metal system, $\beta U^{\rm awm}$ is obtained as

$$\beta U^{\rm awm}(r,L)=2Z^2\kappa\lambda_B\int_0^\infty\frac{\hat{l}J_0(\kappa rl)}{\coth(\kappa L\tilde{l})+\epsilon_{12}\hat{l}}dl. \quad (11)$$

Case III: Air-water-air (AWA) system. Here, $\chi_{12}=\chi_{23}$. This situation would ideally represent particles suspended in a thin film of water in air. It would also model systems where the ϵ_3 substrate is a low polarizability medium ($\epsilon_3\sim1\to6$)

where the ratio ϵ_{32} is of the same order as ϵ_{12}. The pair potential $\beta U^{\mathrm{awa}}(r,L)$ for this system is obtained as

$$\beta U^{\mathrm{awa}}(r,L)=2Z^2\kappa\lambda_B\int_0^\infty J_0(\kappa r l)\left(\frac{\epsilon_{12}\hat{l}\tanh(\kappa L\tilde{l})+1}{\tanh(\kappa L\tilde{l})+2\epsilon_{12}\hat{l}}\right)dl. \tag{12}$$

Case IV: Air-water-water (AWW) system. In this case, $\epsilon_2=\epsilon_3$ so that $\chi_{23}=(\tilde{l}-l)/(\tilde{l}+1)$. This represents a hypothetical situation where the substrate is of the same dielectric material as water but without mobile charges. It exposes the effect of the confining substrate on the interaction without image-charge forces. The pair potential is obtained as follows:

$$\beta U^{\mathrm{aww}}(r,L)=2Z^2\kappa\lambda_B\int_0^\infty J_0(\kappa r l)\times\left(\frac{\tanh(\kappa L\tilde{l})+1/\hat{l}}{(1/\hat{l}+\epsilon_{12}\hat{l})\tanh(\kappa L\tilde{l})+\epsilon_{12}+1}\right)dl. \tag{13}$$

The potentials above are still in their integral forms. Unfortunately, they cannot be performed analytically. We have therefore performed the integrals numerically in order to capture sufficient details in the electrostatic interaction. Figures 2(a)–2(c) show the variation of the pair potentials with the pair separation, κr for various interfaces' separation distances κL. The full solid curve is for the AW system, Eq. (7) (no substrate) corresponding to $\kappa L=\infty$ for any of the other cases: βU^{awm}, βU^{awa}, and βU^{aww} for the AWM, the AWA, and the AWW systems, respectively. The latter [AWW, Fig. 2(a)] is plotted to show the small but finite effect of pure confinement without any dielectric change across the substrate-water interface. The plots clearly show how the pair interaction between two ions trapped at an air-water interface is modified by bringing a substrate from the bulk of the solution to a finite distance from the air-water interface. Of particlar interest is the opposing effects of the two extreme classes of substrates being investigated. While decreasing the AWA interfaces' separation κL enhances the repulsive pair interaction [Fig. 2(b)], the effect of the same action for the AWM system is weakening the repulsive interaction, becoming very short ranged for very small κL [Fig. 2(c)].

This behavior can be explained with electrostatic image-charge forces [35]. The total electrostatic potential due to an ion in a medium of dielectric constant, say ϵ, near another medium of dielectric constant, say ϵ', is the sum of the potential due to its real charge q and that due to its image charge, $q'=q(\epsilon-\epsilon')/(\epsilon+\epsilon')$. If the ϵ medium is, for example, water and the ϵ' medium is air so that $\epsilon>\epsilon'$, then q' is of the same sign as q and the total potential due to both charges doubles in magnitude with respect to the bulk value (absence of interface) for a point at the interface. On the other hand, if the ϵ' medium is a metallic substrate and the ϵ medium is still water, $\epsilon<\epsilon'=\infty$ and the image charge is equal in magnitude and opposite in sign to the real charge.

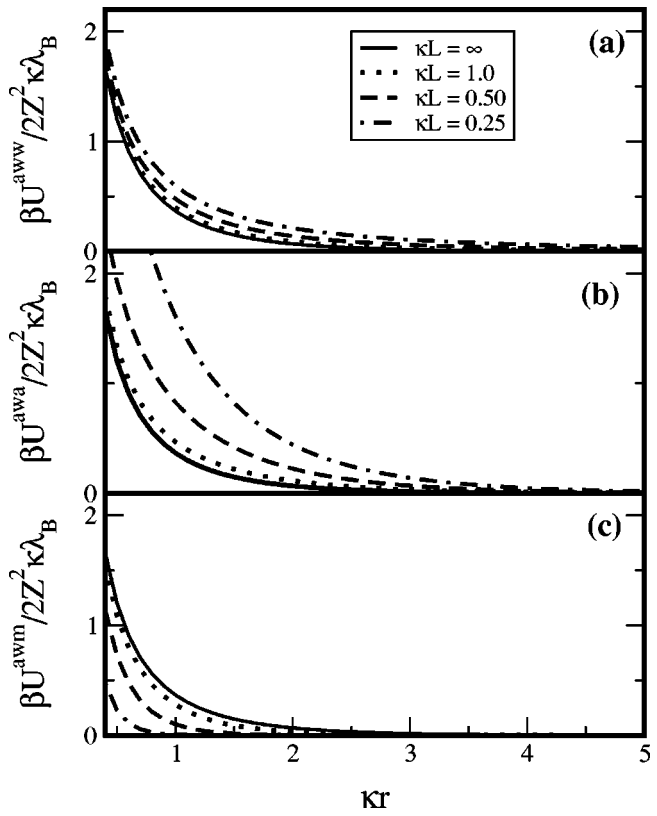

FIG. 2. Linear plot of the pair potentials versus pair separation distance κr for the various systems of interfaces: (a) the air-water-water (AWW), Eq. (13); (b) the air-water-air (AWA), Eq. (12); and (c) the air-water-metal (AWM), Eq. (11). The solid line, $\kappa L=\infty$, corresponds to the air-water only (AW) system, Eq. (7).

The potential in this case is subtractive and vanishes for any point on the metal substrate. Electrostatic screening of charges by electrolyte ions does not change this picture qualitatively, but leads just to an additional factor $e^{-\kappa r}$ in the potential [34]. Now, for our case with two point charges at the air-water interface, this implies that one point charge (the test charge) sees the potential of two other charges, namely, the real charge $+Ze$ at $z=0$ and its image charge $-Ze$ $(+Ze)$ at $z=2L$ in the AWM system (AWA system), respectively. The electrostatic potential at the position of the test charge and thus the interaction potential then reduces in the AWM system and increases in the AWA, relative to the value it has in the absence of a substrate.

Figure 2 is plotted only up to a few κr. To reveal the full range functional behavior of the potentials, we replot Fig. 2 in log-log scale up to $\kappa r=20$. The result is Figs. 3(a) and 3(b) for only the AW, AWA, and AWM setups. The plots show for various κL, dominant exponential decay at short pair separations and algebraic decay at large separations, in agreement with Hurd [21]. The u^{yuk} $(=\beta U^{\mathrm{yuk}}/2Z^2\kappa\lambda_B)$ of Eq. (8) is included to show the deviation of the potentials from a pure Yukawa-like potential decay.

We have thus established that the presence of an additional interface has both qualitative and quantitative effect on the pair interaction of macroions at an air-water interface. In what follows, we are going to probe these potentials further

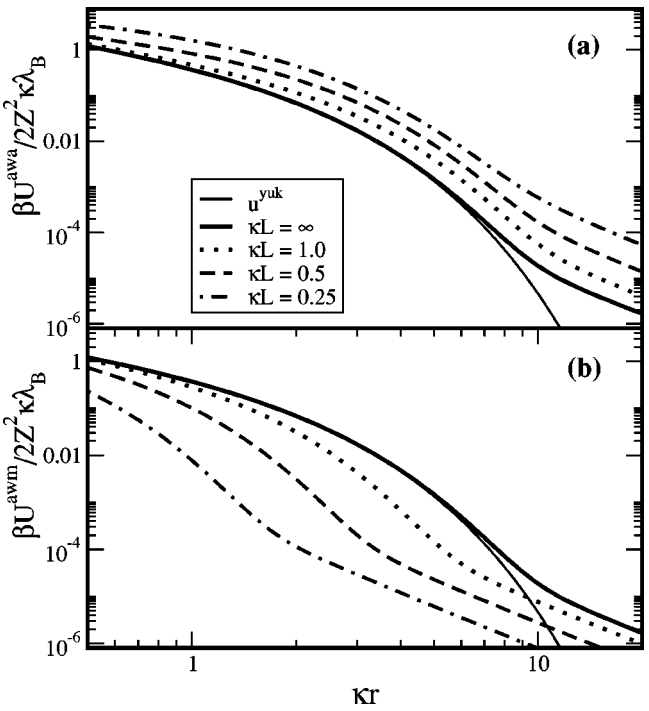

FIG. 3. Log-log plot of the pair potentials versus pair separation for (a) the AWA system and (b) the AWM system. The thin solid line u^{yuk} is the pure Yukawa exponential decay, Eq. (8).

for structural effects on two-dimensional colloidal suspension of particles trapped at an air-water interface via MC simulation.

III. MODELS AND SIMULATION DETAILS

Good fits of the pair potentials, Eqs. (7), (11), and (12), have been made to obtain energy parameters used in the canonical ensemble MC simulation of the quasi-2D system of colloidal particles trapped at an air-water interface with and without additional substrate interface. The fit formulas are of the general form for the reduced potential,

$$u(\kappa r,\kappa L)=\frac{b_1 e^{-b_2\kappa r}}{(\kappa r)^{b_3}}+\frac{b_4}{(\kappa r)^{b_5}}, \tag{14}$$

where $u(\kappa r,\kappa L)=\beta U(\kappa r,\kappa L)/2Z^2\kappa\lambda_B$. Values of the parameters b_i $(i=1,2,3,4,5)$ for various different values of κL and for the three systems AWM, AWA, and AW are listed in Table II.

In the simulation, the particles are no longer taken to be pointlike ions, but have finite size of diameter $2a$. Hence, the density of the 2D system of particles is best described by the particle surface fraction $\phi_{surf}=\pi a^2\rho$, where $\rho=N/S_{box}$ is the number density, with N the total number of the particles in the simulation box of surface area S_{box}. The appropriate pair interaction then includes a hard-core part,

$$\beta V(r)=\begin{cases}\infty, & r<2a\\ 2Z^2\gamma^2\lambda_B\kappa u(\kappa r,\kappa L), & r\geqslant 2a.\end{cases} \tag{15}$$

Furthermore, the introduction of finite size for the macroions demands the familiar DH correction of the total charge Z in the form $Z\rightarrow Z\gamma$ where $\gamma=e^{\kappa a}/(1+\kappa a)$. The validity of this correction in the present situation is doubtful since only a half of the particle surface is assumed immersed in the aqueous phase and hence only this part carries surface charges. But since for the sizes of colloidal particles being considered here, the factor γ makes only a small difference, we will leave it at that. It is convenient to work with reduced units. We take a as the unit length scale in the following. Then the independent parameters of our calculation are ϕ_{surf}, $\Lambda\equiv Z^2\lambda_B/a$, $\zeta\equiv\kappa a$, and L/a, and Eq. (15) becomes

$$\beta V(r/a)=\begin{cases}\infty, & r/a<2\\ 2\Lambda\gamma^2\zeta u(\zeta r/a,\zeta L/a), & r/a\geqslant 2.\end{cases} \tag{16}$$

In all simulation runs, the 2D rectangular simulation box, with aspect ratio $2:\sqrt{3}$ contained a total of $N=1024$ particles. The preferred aspect ratio makes the box a unit cell of the target crystal structure (triangular lattice). This minimizes the influence of the simulation box upon the structure of the system. We varied the surface fraction ϕ_{surf} only up to 2%, where the average particles' separation distance is about six particle diameters, thus remaining in the low concentration regime. Particles were moved only in the lateral x-y directions with periodic boundary conditions according to the standard Metropolis algorithm [36]. Each starting configuration consisted of particles uniformly distributed over the simulation box on a triangular lattice. The systems were equilibrated with about 20000–50 000 MC cycles by monitoring the energy. One MC cycle corresponds to N $(=1024)$ attempted moves of a particle. About 5000 to 10 000 MC cycles were used to obtain the statistical averages of the density dependent quantities characterizing the particle structures at the interface. These quantities are the bond-orientational order parameter Φ_6, the 2D pair-correlation function $g(r)$, and the orientational correlation function $g_B(r)$, introduced in the following.

The order parameter Φ_6 was introduced by Nelson and Halperin [37] to characterize the structural order in 2D systems. It is viewed as the absolute value of the sixth Fourier component of the bond angle distribution function, which is constant in the isotropic fluid and consists of six equally spaced peaks in the solid phase. It is given by [11,38]

$$\Phi_6=\left\langle\frac{1}{N}\sum_{m=1}^{N}\frac{1}{N_b}\sum_{n=1}^{N_b}e^{6i\theta_{mn}}\right\rangle. \tag{17}$$

The angular brackets indicate the configurational average and θ_{mn} is the angle between some fixed axis (e.g., x or y axis) and the bond joining the mth particle with another nth neighboring particle, and N_b denotes the number of such particle-neighbor bonds. Various definitions of particle-neighbor distances have been given in the literature, but as long as the shell of the next-nearest neighbors is excluded, details of the neighborhood definition have a negligible influence on the results [39]. In this present work, we declare two particles as neighbors if their center-center separation is equal or less than $d_{nn}=1/\sqrt{\rho}$, the mean separation between

particles in a system of number density ρ. The square of the absolute value of the bond-orientational order parameter $|\Phi_6|^2$ is used to characterize the structural order of the system [31]. When the system belongs to the fluid phase, $|\Phi_6|^2 \ll 1$. On the other hand, $|\Phi_6|^2 \sim 1$ when the particles form perfect crystalline order of triangular lattice structure.

For further clarification on the structure and phase behavior of the systems, the pair-correlation function $g(r)$ and the orientational correlation function $g_B(r)$ are also determined by MC simulation. The $g(r)$ determines the translational order of the particles and is defined as [40]

$$g(r) = \langle \delta(\mathbf{r}')\,\delta(\mathbf{r}'-\mathbf{r})\rangle = \left\langle \frac{S_{\text{box}}}{N^2} \sum_i \sum_{j>i} \delta(\mathbf{r}-\mathbf{r}_{ij}) \right\rangle, \tag{18}$$

where S_{box} is the 2D volume of the simulation box. On the other hand, the particles' bond-orientational order is determined by the $g_B(r)$ defined as [41],

$$g_B(r) = \langle \psi_6^*(\mathbf{r}')\,\psi_6(\mathbf{r}'-\mathbf{r})\rangle / \langle \delta(\mathbf{r}')\,\delta(\mathbf{r}'-\mathbf{r})\rangle = \left\langle \sum_i \sum_{j>i} \psi_6(\mathbf{r}_i)\,\psi_6^*(\mathbf{r}_j)\,\delta(\mathbf{r}-\mathbf{r}_{ij}) \right\rangle / g(r), \tag{19}$$

where $\psi_6(\mathbf{r}_m)$, $m \equiv i,j$ is the local bond-orientational order parameter

$$\psi_6(\mathbf{r}_m) = \frac{1}{N_b} \sum_{n=1}^{N_b} e^{6i\theta_{mn}}. \tag{20}$$

The bond-orientational correlation function is used to identify the hexatic phase where a system possesses short-range translational order but a quasi-long-range orientational order, being intermediate between the solid crystal phase and the fluid phase. The region in parameter space of existence of the hexatic phase in most systems is often very narrow. Hence, in order not to lose focus on the main aim of this study, we will not pay much attention in identifying this intermediate phase.

IV. RESULTS AND DISCUSSION

A. Latex particles

From the equilibrium states of the various systems studied (AW, AWA, and AWM), we investigate the concentration dependence of the squared bond-orientational order parameter $|\Phi_6(\phi_{\text{surf}})|^2$, as well as the pair-correlation function $g(r)$ and the bond-orientational correlation function $g_B(r)$, with a view to understanding the electrostatic influence of supporting substrates on the structural behavior of charged particles trapped at an air-water interface.

Figure 4 shows the variation of the order parameter $|\Phi_6|^2$ with the surface fraction ϕ_{surf}. The two outer curves correspond to fixed distances $L/a = 4.0$ in the AWA and AWM systems, while the middle curve corresponds to particles of the AW system ($L \to \infty$) in the absence of any additional interface. The other two parameters are fixed at $\Lambda = 3433$ and $\kappa a = 0.25$. These parameters are typical of latex particles in highly deionized water (for example: $\kappa^{-1} = 200$ nm, $a = 50$ nm, $\lambda_B = 0.72$ nm, and $Z = 500$). Any other possible combination of the parameters leading to the same values for Λ and κa will lead to the same result.

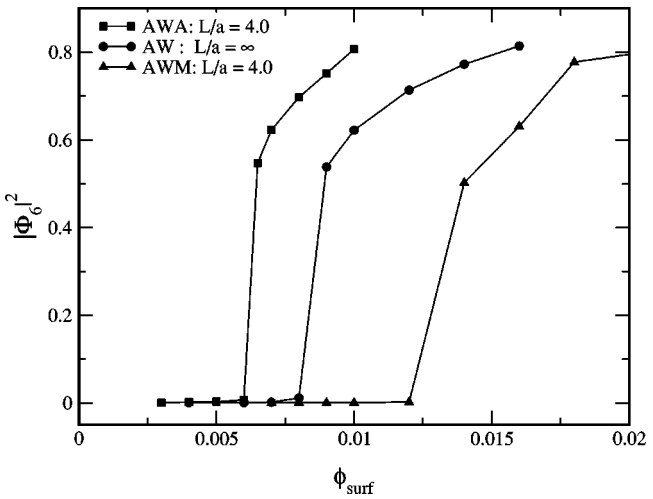

FIG. 4. The square of the orientational order parameter $|\Phi_6|^2$ versus the particle surface fraction ϕ_{surf} for the air-water only system (AW), the air-water-air (AWA), and the air-water-metal (AWM) systems when the reduced interfaces separation distance L/a is held at 4.0. Other fixed parameters are $\Lambda = 3433$ and $\kappa a = 0.25$.

In all three curves, we see that $|\Phi_6|^2 \sim 0$ for a range of colloid densities, indicating that the systems belong to the fluid phase. Then there is a critical density at which the system experiences a jump in the order parameter (to $|\Phi_6|^2 \approx 0.5$) when the system makes transition to crystalline phase. This $|\Phi_6|^2$ behavior is quite in agreement with that presented in Ref. [11]. The substrate-water interface again as in the case of the interaction potentials shows opposing effects in going from the AWA system to AWM system with respect to AW system. The AWA system exhibits crystals at densities (lower) where the AW and AWM systems shows fluid structures, obviously due to the enhanced repulsive pair-interaction potential for the AWA system observed in Fig. 2. That is, bringing a metallic surface near to the 2D system at the air-water interface induces a shift of the freezing density to higher densities. This shows that, and how the additional dielectric substrate affects the crystallization behavior of the 2D colloidal system.

To further expose the distinct effects of the two classes of interfaces, we characterize in Fig. 5 the structural features of the systems (parameters as in Fig. 4) at an arbitrary reference surface fraction, $\phi_{\text{surf}} = 0.008$. Figure 5 shows, (a) equilibrated configuration snapshots of the particles, (b) the pair-correlation functions $g(r)$, and (c) the orientational-correlation function $g_B(r)$, for the three systems—(i) AWA, $L/a = 4.0$, (ii) AW, $L/a = \infty$, and (iii) AWM, $L/a = 4.0$. The figure reveals that at the reference density $\phi_{\text{surf}} = 0.008$ the AWA system displays clearly a solid phase from the $g(r)$ with quasi-long-range translational order, and crystalline order from point of view of $g_B(r)$ with finite and long-ranged nondecaying values. At the same density, the AWM system shows an isotropic fluid phase where both $g(r)$ and $g_B(r)$

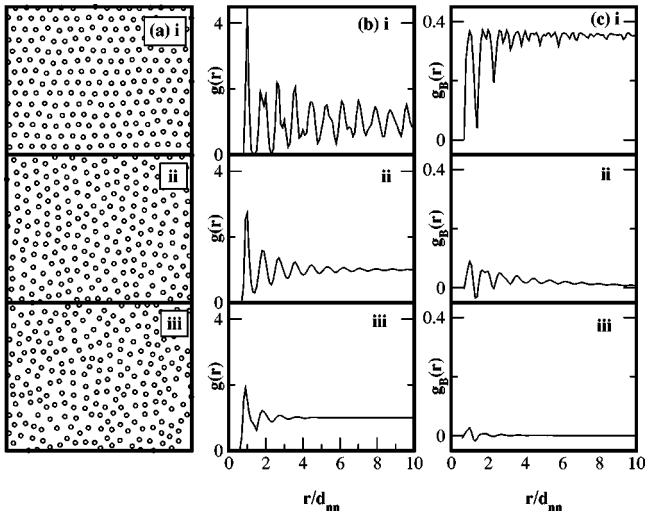

FIG. 5. Two-dimensional structural characterization of the particles trapped at the air-water interface at $\phi_{\mathrm{surf}}=0.008$. The columns; (a) snapshots, (b) the pair-correlation function $g(r)$, and (c) the bond-orientational correlation function $g_B(r)$; and the rows: (i) the AWA system ($L/a=4.0$), (ii) the AW system ($L/a=\infty$), and (iii) the AWM system ($L/a=4.0$). Other fixed parameters are as in Fig. 4. $d_{nn}=\sqrt{\rho}$ is the mean interparticle distance at the given density $\rho=\phi_{\mathrm{surf}}/\pi a^2$.

display short-range order. The snapshots directly clarify these features. An intermediate behavior between the AWA and AWM systems is displayed by the AW system at the same surface fraction. In this system, while the $g(r)$ shows a short-range order, $g_B(r)$ appears quasilong ranged, showing a slow decay to zero. This behavior can be an evidence (but not a rigorous proof) of the existence of a hexatic phase in the melting transition of a 2D colloidal suspension at the air-water interface as investigated in Ref. [11]. We emphasize again that we are not set here to identify the hexatic phase, but rather to show the clear transition to fluid or crystalline orders due to the substrates.

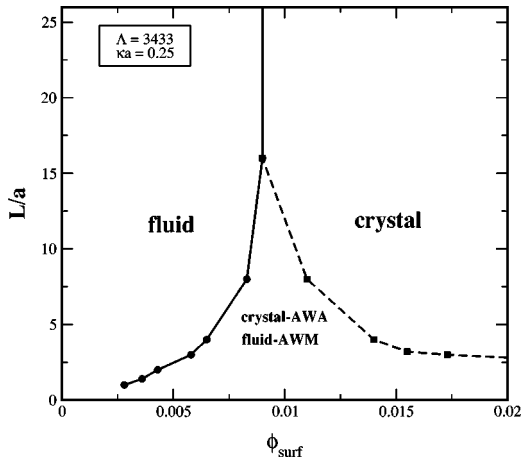

FIG. 6. Phase diagram in the [ϕ_{surf}:L] plane for a set of system parameters corresponding to $\Lambda=3433$ and $\kappa a=0.25$. The regions of the indicated phases are: isotropic fluid phase (*fluid*), crystalline solid phase (*crystal*), and either of both phases depending on the dielectric nature of the additional supporting substrate. In the AWA system, this region is crystalline (*crystal-AWA*), while it is fluid in the AWM system (*fluid-AWM*).

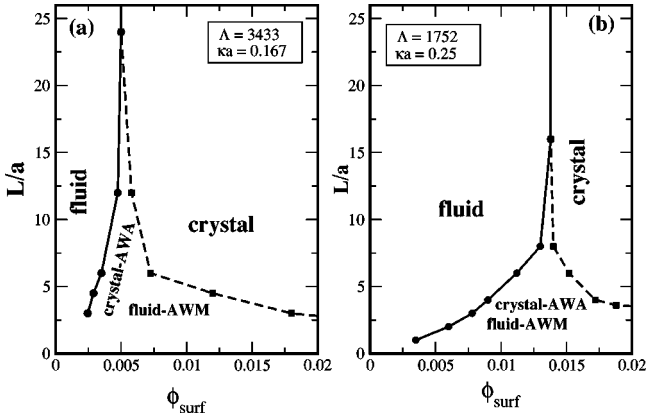

FIG. 7. Same as in Fig. 6 but (a) κa is decreased from 0.25 to 0.167—the region of the crystal phase increases in area; and (b) Λ is decreased from 3433 to 1752—the fluid phase region gains area.

In what follows, we will not invest much effort in locating the exact transition density from the isotropic fluid phase to the crystalline solid phase, or vice versa, often achieved by the cummulant method [39]. We will rather assume that transition occurs at around the jump in $|\Phi_6|^2$, i.e., at values of ϕ_{surf} corresponding to $|\Phi_6|^2\approx 0.5$, which is reasonable from the point of view of Fig. 4 discussed. Figure 6 is a phase diagram based on our model, obtained with the above criterion by systematically calculating $|\Phi_6|^2$ as a function of ϕ_{surf} as in Fig. 4, for varying values of L/a. In this diagram, the reduced parameters are again $\Lambda=3433$ and $\kappa a=0.25$. The figure shows in what regions of the lines drawn for the two systems, AWA and AWM, one expects to find the fluid phase, ''fluid'' and the crystalline solid phase, ''crystal.'' The region labeled ''crystal AWA'' and ''fluid AWM'' belongs to the crystal phase for the AWA system and to the fluid phase for the AWM system. It is seen that at large L, the two lines join into one with values equal to those obtained for the AW system.

Figure 7 shows the effect of changing the reduced parameters, Λ and κa. In Fig. 7(a), Λ is as in Fig. 6, while κa is decreased to 0.167. This could imply, for example, reduction in screening by reducing the ionic strength of the electrolyte ($\kappa^{-1}=300$ nm, $a=50$ nm), or slightly smaller particles ($\kappa^{-1}=200$ nm, $a=33$ nm). Again this leads to stronger repulsive interaction and the effect on the phase diagram is a quantitative shift in favor of the crystal phase. In Fig. 7(b), $\kappa a=0.25$ as in Fig. 6 but Λ takes a smaller value 1752, producing again a shift in the phase diagram but now in favor of the fluid phase.

B. Protein particles

In the light of the results of the preceding section, we extend the simulations to parameters relevant to protein particles at an air-water interface. Some protein particles studied at the air-water interface are known to be of the order of a few nanometers in dimensions and carry quite small numbers

TABLE I. Some proteins particles studied at the air-water interface with some relevant properties and sources.

Protein particle	Tertiary structure	Dimensions (nm×nm×nm)	Hydrodynamic radius (nm)	Charge (pH)	Reference
Lysozyme	globular	4.5×3.0×3.0	1.967	+9(7.0), +12(3.5)	[42], [43]
BSA[a]	globular	14.0×3.8×3.8	3.579	−17(7.0)	[42]
β-casein	disordered coil		3.579	−13(7.0)	[42]
Myoglobin	globular	4.4×4.4×2.5		+19(3.5), −5(9.5)	[43]
Ribonuclease	globular	3.8×2.8×2.2		+13(3.5)	[43]
Apoferritin[b]	globular		6.000	undetermined	[44]/ [45]

[a]Bovine serum albumin.

[b]Apoferritin is the protein ferritin with a spherical core about 6 nm in diameter containing iron oxide [45].

of charges. The net charge on a protein particle is pH dependent and can be varied from negative to positive, taking a vanishing value at the isoelectric point of the protein solution. See Table I for a summary of a few proteins and some of their relevant properties. We investigate again the possible influence of a supporting substrate on the phase behavior of protein particles at the air-water interface. Table I shows that the electrostatic coupling quantity Λ will be quite small for any realistic combination of the composite parameters, compared to values obtained for the latex particles. The observed shift of the phase boundaries in going from a high value of Λ in Fig. 6 to a lower one in Fig. 7(b) suggests that crystallization in 2D protein systems will set in at much higher surface fractions than in colloidal systems. This, we see from Table I, is essentially due to the low net charge carried by proteins. We will therefore focus only on the AWA model, which according to the results on latex particles enhances crystallization and therefore provides the only possible chance of finding the crystal phase at reasonable particle densities.

In the simulations, we probed $\Lambda=87.54$ and 171.42. The former value could correspond to $2a=7.0$ nm, $Z=20$, and $\lambda_B=0.766$ nm (water: $T=278$ K, $\epsilon_2=78.3$), while the latter is obtained by increasing λ_B to 1.5 nm assuming a lower polarizability solution of dielectric constant, $\epsilon_2\approx 40.0$. This assumption is not unreasonable considering that in experiments of protein crystallization, the protein solution is often a concoction whose resultant dielectric constant will be well below that of water. However, the AWA acronym will still be used to describe the resulting air-solution-air system. For $\epsilon_2=40$, a different set of fit parameters must be obtained and are shown also in Table III in the Appendix. For salt concentrations typical of protein solutions [42,43], we fixed κa at 0.175.

Figure 8(a) shows the variation of the order parameter $|\Phi_6|^2$ with the surface fraction $\phi_{\rm surf}$ when the AWA interfaces' separation distance L is equal to the particle radius ($L/a=1.0$). The figure shows that with $\Lambda=87.54$, the protein particles could not form a crystal for the range of surface fraction considered. But increasing Λ to 171.4, the order parameter performs the characteristic jump (here at $\phi_{\rm surf}=.018$) to a high value, so that one can expect a well defined crystalline structure at $\phi_{\rm surf}=0.02$ at the air-solution interface. Figure 8(b) demonstrates that the crystalline order existing at the surface fraction, $\phi_{\rm surf}=0.02$ in Fig. 8(a) collapses to an isotropic fluid phase with also a sudden dive in the order parameter $|\Phi_6|^2$, when L/a is increased from 1.0. The point on the horizontal axis $L/a=\infty$ corresponds to the AW system (i.e., air-solution only interface).

In Fig. 9, we plot the $[\phi_{\rm surf}:L]$-phase diagram for the

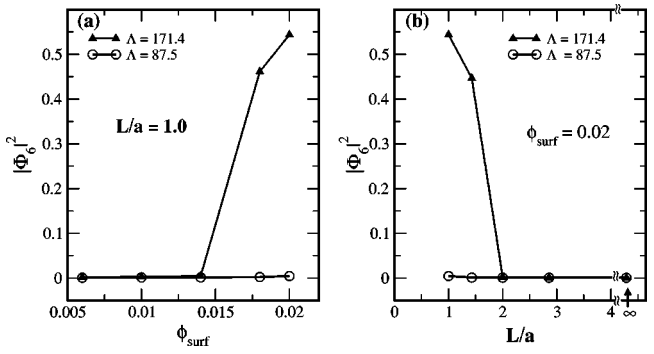

FIG. 8. The order parameter $|\Phi_6|^2$ versus (a) surface fraction $\phi_{\rm surf}$ and (b) air-water–substrate-water separation distance L/a, for sets of parameters appropriate for protein particles at air-solution interfaces as labeled. In both (a) and (b), $\kappa a=0.175$.

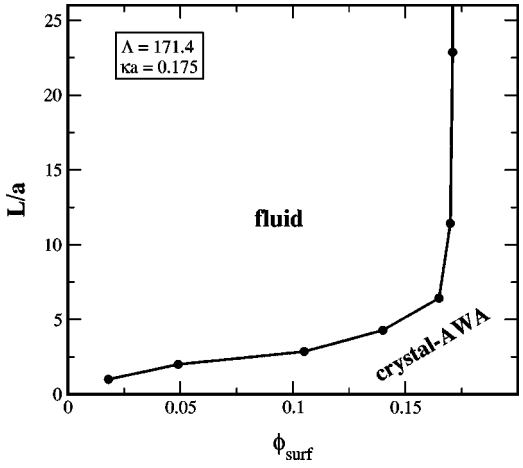

FIG. 9. Phase diagram for a set of system parameters corresponding to $\Lambda=171.4$ and $\kappa a=0.175$ appropriate for protein particles, obtained only for the AWA system.

TABLE II. The fit parameters b_i for $\epsilon_1=1.0$ and $\epsilon_2=78.3$. The values corresponding to κL marked with "*" are obtained for the air-water-air system, "**" are for the air-water-metal system, and $\kappa L=\infty$ is for the air-water only system.

	κr									
	Small separation $\kappa r=0-7$					Large separation $\kappa r=7-\infty$				
κL	b_1	b_2	b_3	b_4	b_5	b_1	b_2	b_3	b_4	b_5
0.25*	4.36968	1.03332	0.38666	0.05188	1.41822	6.75770	0.79906	1.34639	0.75897	3.20032
0.35*	3.16919	1.06816	0.32458	0.07366	1.87064	4.61932	0.84437	1.16922	0.39803	3.20639
0.50*	2.13406	1.01331	0.39440	0.05023	2.22335	4.72500	0.80606	1.49737	0.16537	3.13671
0.75*	1.30101	0.870893	0.662179	0.02989	2.39797	1.92150	0.91642	0.86393	0.09282	3.20049
1.00*	0.99245	0.77318	0.91866	0.00996	2.51205	1.39635	0.93328	0.78978	0.05493	3.18530
2.00*	0.95501	0.95065	1.01137	0.00543	1.35189	0.76352	0.94202	0.80309	0.02030	3.10277
4.00*	0.98485	0.99191	1.00018	0.00115	1.36693	1.29557	0.90959	1.42098	0.01608	3.07225
∞	0.98395	0.99158	1.00029	0.00126	1.57368	0.81882	1.02088	0.81871	0.02700	3.28884
4.00**	0.98562	0.99227	1.00009	0.00083	1.38556	1.07694	0.98345	1.09445	0.01593	3.07056
2.00**	1.01685	1.03296	0.98923	−0.00379	1.36667	3.47061	1.02433	1.93716	0.01384	3.04663
1.00**	1.23932	1.47238	0.90124	−0.00658	1.46043	102.86300	0.437491	7.39092	0.00796	3.02246
0.75**	1.43582	1.91032	0.83769	−0.00451	1.55401	0.00520	0.58665	2.31473	0.00469	2.95943
0.50**	1.86138	2.89575	0.73788	−0.00177	1.81432	−8.46E−05	0.10370	1.58336	0.0028	2.90339
0.25**	2.84005	5.92461	0.64324	−1.44E−05	5.43621	−4.17E−06	0.21541	0.32290	0.00059	2.76656

protein particles ($\Lambda=171.4$, $\kappa a=0.175$) with the same freezing criteria used for Figs. 6 and 7 in the latex-colloid system. The protein phase diagram while qualitatively identical to the latex particle ones, however shows a much larger region in the $[\phi_{\text{surf}}:L]$ plane for the fluid phase. The system exhibits the crystal phase only at rather high surface densities, about an order of magnitude larger in comparison with densities for the latex particles. Figure 9 reveals how effective the additional substrate now becomes in promoting crystallization: already at relatively large separations of $L/a=5$ one observes a clear shift of the freezing transition point from its original value (no substrate) at about $\phi_{\text{surf}}=0.18$ to $\phi_{\text{surf}}=0.15$, and at $L/a=2.5$ freezing sets in already at $\phi_{\text{surf}}=0.06$, that is, at a protein surface fraction which is a factor of 3 smaller than it is in the unconfined system. Figures 8 and 9 thus demonstrate that, using the model pair interactions described in this work, a low polarizability supporting substrate, whose dielectric constant is much smaller than that of water ($\epsilon_3 \ll \epsilon_2$), is capable of inducing crystallization in an, otherwise, fluid 2D protein system when the separation distance between the substrate and air is comparable to the particle size. We, however, also remark that at such high densities, the average particles' separation distances d_{nn} become comparable to the particles' size. Apart from the technical problem of requiring more particles in the simulation (which demands more computation time), the neglect of the van der Waals forces in the model then becomes certainly less justifiable.

V. SUMMARY AND CONCLUSION

The present study has focused on the question of how to control-influence effective pair interactions and thus the crystallization behavior of a system of charged macro particles trapped at an air-water interface. Conventional ways to tune the effective interactions include changing the salt content, the temperature or the dielectric properties of the solvent. As an alternative method, we here suggest to manipulate the particle interaction via additional dielectric substrates. To study the effect of such an additional substrate, we have considered only three but representative substrate-solution interfaces giving rise to the following systems of interfaces: air-water-metal (AWM), air-water-air (AWA), and air-water-water (AWW). Metal represents media of dielectric constants much higher than water ($\epsilon_{\text{metal}} \sim \infty$), air represents media on the opposite end ($\epsilon_{\text{air}} \sim 1$), while the AWW system

TABLE III. The fit parameters b_i for $\epsilon_1=1.0$ and $\epsilon_2=40.0$ obtained for protein particles in the air-solution-air system.

	κr									
	Small separation $\kappa r=0-7$					Large separation $\kappa r=7-\infty$				
κL	b_1	b_2	b_3	b_4	b_5	b_1	b_2	b_3	b_4	b_5
0.175	5.90557	1.11571	0.30643	0.19672	1.30551	16.69520	0.46874	2.73382	2.20759	3.08202
0.250	4.24392	1.10785	0.29197	0.14138	1.51621	9.89539	0.60330	2.20350	1.26082	3.13354
0.350	2.83067	1.00914	0.38945	0.08782	1.69163	7.10615	0.67153	1.97503	0.67289	3.14514
0.500	1.73127	0.84728	0.60044	0.05126	1.81383	4.73814	0.73498	1.73526	0.34197	3.14931
∞	0.97308	0.98551	1.00007	0.00154	1.14008	2.00690	0.82914	1.92410	0.02845	3.02717

models systems where the substrate is of the same polarizability as the electrolyte (water). Two similarly charged particles at an air-water interface are known to interact via a repulsive electrostatic dipole-dipole potential in addition to the well known Yukawa-like screened Coulomb potential. We showed that the presence of the additional interface results in a modification of the total electrostatic repulsive interaction potential, enhancing it in the case of the AWA system but with a diminishing effect in the AWM system. Applying these model pair-interaction potentials, we investigated via MC simulation the density dependent quasi-2D structural and phase behavior of two classes of colloidal particles, namely, highly charged latex particles and charged protein particles.

In the case of latex particles, we obtained fluid to crystal transition phase diagrams in the particle density-interfaces separation distances plane $[\phi_{\text{surf}}:L]$ for low salt concentrations. While the AWA system facilitates formation of crystals at low particle concentration relative to the air-water only (AW) system, the AWM system behaves otherwise, in accordance with the opposing behavior of their pair-interaction potentials. This then is the essential conclusion of this paper: it is possible to influence the crystallization behavior of 2D systems of charged particles at the air-water interface by an additional dielectric substrate, brought into neighborhood of the air-water interface. This might bear some relevance for protein crystallization in 2D. The positive influence of the AWA system on 2D crystallization of latex particles motivated the extension of the model to investigate 2D crystallization of proteins, where the total charge on the particle is very low ($Z \sim 15$). The protein particles phase diagram obtained showed some sets of system parameters where it is possible to form 2D crystals when the interfaces separation distance, L becomes comparable with the particles' sizes. The results obtained in this study should be insightful enough to guide the experimentalist in choosing materials and substrate interfaces for growing 2D structures, e.g., crystals at air-solution interfaces.

ACKNOWLEDGMENTS

We thank C. Fleck, C. Russ, and R. Klein for helpful discussions and comments. Financial support from the Deutsche Forschungsgemeinschaft (Grant No. SFB 513) is gratefully acknowledged.

APPENDIX A: THE FIT PARAMETERS FOR THE PAIR-INTERACTION POTENTIALS

In Tables II and III, we tabulate for reproductive purposes, the fit parameters b_i, in the fit function

$$f(r,b) = b_1 e^{-b_2(\kappa r)}/(\kappa r)^{b_3} + b_4/(\kappa r)^{b_5},$$

for the interaction potentials $u = \beta U/2Z^2\kappa\lambda_B$ with βU from Eqs. (7), (11), and (12). To obtain very accurate fits for the potentials, it was necessary to separate the pair separation distance κr into small and large.

[1] F. Burmeister, W. Badowsky, T. Braun, S. Wieprich, J. Boneberg, and P. Leiderer, Appl. Surf. Sci. **145**, 461 (1999).
[2] P. Pieranski, Phys. Rev. Lett. **45**, 569 (1980).
[3] G.Y. Onoda, Phys. Rev. Lett. **55**, 226 (1985).
[4] J. Ruiz-Garcia, R. Gamez-Corrales, and B. Ivlev, Physica A **236**, 97 (1997).
[5] A.J. Hurd and D.W. Schaefer, Phys. Rev. Lett. **54**, 1043 (1985).
[6] D.J. Robinson and J.C. Earnshaw, Phys. Rev. A **46**, 2045 (1992).
[7] J. Stankiewicz, M.A. Cabrerizo-Vilchez, and R. Hidalgo-Alvarez, Phys. Rev. E **47**, 2663 (1993).
[8] F. Ghezzi and J.C. Earnshaw, J. Phys.: Condens. Matter **9**, L517 (1997).
[9] R. Kesavamoorthy, C.B. Rao, and B. Raj, J. Phys.: Condens. Matter **5**, 8805 (1993).
[10] J. Ruiz-Garcia and B. Ivlev, Mol. Phys. **95**, 371 (1998).
[11] T. Terao and T. Nakayama, Phys. Rev. E **60**, 7157 (1999).
[12] B. Löhle and R. Klein, Physica A **235**, 224 (1997).
[13] H. Yoshimura, S. Endo, M. Matsumoto, K. Nagayama, and Y. Kagawa, J. Biochem. **106**, 958 (1989).
[14] H. Yoshimura, M. Matsumoto, S. Endo, and K. Nagayama, Ultramicroscopy **32**, 265 (1990).
[15] K. Nagayama, in *Advances in Biophysics*, edited by Setsuro Ebashi (Elsevier, Limerick, 1997), Vol. 34, p. 3.
[16] E.E. Uzgiris and R.D. Kornberg, Nature (London) **301**, 125 (1983).
[17] F.C. Meldrun, B.R. Heywood, and S. Mann, Science **257**, 522 (1992).
[18] P.A. Kralchevsky and N.D. Denkov, Curr. Opin. Colloid Interface Sci. **6**, 383 (2001).
[19] P. A. Kralchevsky and K. Nagayama, *Particles at Fluid Interfaces and Membranes: Attachment of Colloid Particles and Proteins to Interfaces and Formation of Two Dimensional Arrays* (Elsevier, Amsterdam, 2001).
[20] P.A. Kralchevsky and K. Nagayama, Adv. Colloid Interface Sci. **85**, 145 (2000).
[21] A.J. Hurd, J. Phys. A **18**, L1055 (1985).
[22] R. Aveyard, J.H. Clint, and V.N. Paunov, Langmuir **16**, 1969 (2000).
[23] A.S. Dimitrov, T. Takahashi, K. Furusawa, and K. Nagayama, J. Phys. Chem. **100**, 3163 (1996).
[24] T. Takahashi, A.S. Dimitrov, and K. Nagayama, J. Phys. Chem. **100**, 3157 (1996).
[25] K. Zahn, R. Lenke, and G. Maret, Phys. Rev. Lett. **82**, 2721 (1999).
[26] P.A. Kralchevsky and K. Nagayama, Langmuir **10**, 23 (1994).
[27] F. Martínez-López, M.A. Cabrerizo-Vílchez, and R. Hidalgo-Álvarez, J. Colloid Interface Sci. **232**, 303 (200).
[28] E.C. Mbamala and H.H. von Grünberg, J. Phys.: Condens. Matter **14**, 4881 (2002).
[29] E. Chang and D. Hone, J. Phys. (France) **49**, 25 (1988).
[30] H. Löwen, J. Phys.: Condens. Matter **4**, 10 105 (1992).

[31] J. Chakrabarti and H. Löwen, Phys. Rev. E **58**, 3400 (1998).
[32] R.R. Netz, Eur. Phys. J. E **3**, 131 (2000).
[33] S.L. Carnie and D.Y.C. Chan, Mol. Phys. **51**, 1046 (1984).
[34] F.H. Stillinger, J. Chem. Phys. **35**, 1584 (1961).
[35] J.N. Israelachvili, *Intermolecular and Surface Forces* (Academic Press, London, 1992).
[36] N. Metropolis, A.W. Rosenbluth, M.N. Rosenbluth, A.N. Teller, and E. Teller, J. Chem. Phys. **21**, 1087 (1953).
[37] D.R. Nelson and B.I. Halperin, Phys. Rev. B **19**, 2457 (1979).
[38] M.S.S. Challa, D.P. Landau, and K. Binder, Phys. Rev. B **34**, 1841 (1986).
[39] H. Weber, D. Marx, and K. Binder, Phys. Rev. B **51**, 14 636 (1995).
[40] M.P. Allen and D.J. Tildesley, *Computer Simulation of Liquids* (Clarendon Press, Oxford, 1987).
[41] A.H. Marcus and S.A. Rice, Phys. Rev. E **55**, 637 (1996).
[42] T. Sengupta and S. Damodaran, Langmuir **14**, 6457 (1998).
[43] J.J. Bergers *et al.*, Biochemistry **32**, 4641 (1993).
[44] T. Furuno, H. Sasabe, and K.M. Ulmer, Thin Solid Films **180**, 23 (1989).
[45] H. Yoshimura, T. Scheybani, W. Baumeister, and K. Nagayama, Langmuir **10**, 3290 (1994).